

StarSD: One-for-Many Speculative Decoding

Junhao He¹ Feiran You¹ Hongyang Du¹

Abstract

Speculative decoding accelerates autoregressive generation by separating token proposal from verification, but most existing approaches are designed for single-node execution and do not scale well to multi-accelerator clusters used for serving modern Large Language Models (LLMs). We present StarSD, a one-for-many speculative decoding framework that uses a single draft model to serve multiple target models across distributed nodes via a star topology. StarSD decouples drafting and verification, enabling effective sharing of draft computation, and preventing distributed accelerators from remaining idle under bursty workloads. We provide a system-level analysis that characterizes when and why a single draft model can remain fully utilized by multiple verifiers, yielding predictable latency and utilization gains. Extensive experiments in real-world distributed inference settings demonstrate that StarSD simplifies deployment and supports flexible resource allocation across heterogeneous accelerators, while maintaining output quality. These results indicate that StarSD is a practical and scalable framework for bringing speculative decoding to modern cloud and edge inference infrastructures.

1. Introduction

Large Language Models (LLMs) have become a central interface for a wide range of applications, and their deployment increasingly involves serving large volumes of concurrent inference requests in shared accelerator clusters. Under such workloads, inference systems face sustained pressure on latency, throughput, and hardware efficiency, often operating near the limits of memory and compute. A key source of this pressure is *autoregressive* decoding, where each output token requires a serial forward pass, directly constraining end-to-end latency and limiting achievable throughput.

¹Department of Electrical and Electronic Engineering, The University of Hong Kong, Hong Kong SAR, China. Corresponding author: Hongyang Du <duhy@hku.hk>.

Preprint. January 30, 2026.

This bottleneck has motivated many decoding acceleration methods that restructure generation to reduce the cost of sequential decoding. Among them, speculative decoding offers a *lossless* acceleration approach by introducing a lightweight *draft* model to propose multiple tokens that a large *target* model verifies in parallel, preserving the target model’s output distribution while reducing decoding time (Leviathan et al., 2023; Chen et al., 2023). Unlike batching or approximate decoding, this separation mechanism preserves exact generation semantics while exposing additional parallelism, which makes speculative decoding suitable for latency-sensitive serving. Building on this advantage, several methods are proposed to improve draft quality and reduce verification costs, thereby further increasing acceptance rates and achieving decoding speedups (Li et al., 2024a; Miao et al., 2024; Li et al., 2024b).

However, most speculative decoding designs implicitly adopt a centralized execution mode, in which the draft and target models are co-located on a single accelerator, e.g., a Graphics Processing Unit (GPU). This pattern is increasingly misaligned with production inference systems, as modern LLMs continue to grow in parameter scale and deployment workloads impose sustained memory pressure through large Key-Value (KV) caches, causing the combined footprint to approach or even exceed the capacity of a single accelerator. For instance, co-locating a Vicuna-7B (Zheng et al., 2023) target model with the lightweight EAGLE draft model can leave little memory headroom (Li et al., 2024a) for an RTX 4090 (24GB), restricting support for long-context serving. Moreover, as LLMs expand into vertical domains and are increasingly deployed on resource-constrained edge devices, e.g., PCs, mobile phones, or NVIDIA Jetson, co-location becomes even less practical due to tighter memory and compute budgets. Although substantial work has explored memory-efficient inference techniques (Kwon et al., 2023; Sheng et al., 2023), these methods do not remove the need to host the target-draft model pair on every accelerator, which constrains batching efficiency and scheduling flexibility.

Consequently, LLM inference systems require a spatial degree of freedom, enabling distributed placement that allows drafting and verification to be placed independently while cooperating tightly to share accelerator resources. In principle, this flexibility supports higher utilization by decoupling

compute-intensive drafting from request-driven verification, and applies both within a single server across multiple accelerators and distributed clusters across machines. However, simply separating the draft and target models reveals an accelerator-level inefficiency due to a mismatch between the model inference pattern and the operating characteristics of modern accelerators. Specifically, the draft-then-verify workflow alternates between drafting, verification, and communication, while the target model verifies proposed tokens, the draft model remains idle. This alternating execution introduces *idle gaps* that limit end-to-end throughput. In addition, disaggregation makes the draft execution *bursty*, with short compute phases separated by millisecond-scale gaps. Such bursty execution can prevent the draft model from staying in a warm compute state, increasing per-token latency and its variance compared to continuous execution.

Addressing these challenges requires a novel speculative decoding framework that can coordinate drafting and verification across machines while sustaining steady execution on modern accelerators. We propose StarSD, a one-for-many distributed speculative decoding framework where a single draft model concurrently assists multiple target instances. StarSD multiplexes asynchronous returns through a global request buffer and executes requests in a work-conserving loop with per-instance state isolation, ensuring continuous utilization of the draft accelerator whenever work is available. To analyze performance under concurrency, we develop an analytical system model that decouples *progress*, measured as the expected number of accepted tokens per round, from *time*, measured as the round duration. The model characterizes under-loaded and fully-loaded regimes and identifies the transition point at which idle gaps vanish.

StarSD yields two complementary benefits under multi-instance workloads. By amortizing verification and communication return latency across multiple targets, it reduces idle gaps and increases aggregate throughput. Furthermore, a continuous request stream keeps the draft side closer to a steady-state execution regime, improving draft-side per-token compute efficiency and stability. These effects make speculative decoding more effective in disaggregated and memory-constrained deployments without changing model weights or the output distribution. Our contributions are summarized as

- We propose StarSD in the one-for-many distributed speculative decoding setting, a framework that isolates per-target state and enables work-conserving draft execution in the presence of asynchronous verification returns from targets.
- We develop an analytical system model that separates per-iteration progress from per-iteration time, characterizes load regimes, and explains scaling behavior,

saturation effects, and the tradeoff between per-target throughput and system-wide throughput.

- We evaluate StarSD across various deployments, including intra-machine multi-GPU, inter-machine multi-GPU, and heterogeneous platforms such as a Computer-Jetson setup. The results show that StarSD scales throughput with the number of target instances until saturation, with continuous drafting reducing per-token compute time and latency variance compared with bursty execution.

2. Preliminary

Speculative decoding speeds up autoregressive inference by splitting decoding into two roles, i.e., a lightweight *draft* model proposes candidate continuations, and a large *target* model verifies them. Following the original speculative decoding formulation (Leviathan et al., 2023), we denote the target and draft model types by \mathcal{M}_p and \mathcal{M}_q , and use M_p and M_q to refer to their deployed instances, respectively. When StarSD serves N target instances concurrently, we index them as $\{M_p^{(i)}\}_{i=1}^N$. In the single-instance case, we drop the index and write $M_p \equiv M_p^{(1)}$ for notational simplicity.

Per-request primitive. Given a verified prefix, one speculative decoding step contains of two stages: (i) **proposal**, where the draft instance M_q generates candidate continuations from the prefix, and (ii) **verification**, where the target instance M_p verifies the proposals and returns an *accepted prefix* defined as the longest prefix that passes verification. Both models then advance to the accepted prefix and continue decoding.

Tree-based proposals. SpecInfer (Miao et al., 2024) popularizes *tree-based* speculative proposals to better exploit accelerator parallelism. Rather than proposing a single token chain, M_q expands a token tree of depth d with branching factor k , i.e., top- k candidates per step, so that the target model can score many candidate continuations in parallel within a batched forward pass. Following this design, advanced systems such as EAGLE (Li et al., 2024a) adopt tree-style expansion to increase the likelihood of finding a long verifiable prefix while maintaining high verification throughput. In this work, we also adopt the tree-based drafting and use the depth d to parameterize the draft workload.

Acceptance intuition. The number of accepted tokens mainly depends on how well \mathcal{M}_q matches \mathcal{M}_p under the current prefix. A smaller draft-target mismatch typically yields longer accepted prefixes. Beyond architectural designs, several works explicitly align \mathcal{M}_q to \mathcal{M}_p via training, e.g., DistillSpec (Zhou et al., 2023) and AdaSPEC (Hu et al., 2025) use distillation tailored to speculative decoding, while Online Speculative Decoding (Liu et al., 2023) reduces mismatch after deployment by periodically updating \mathcal{M}_q using

the corrections from \mathcal{M}_p . EAGLE (Li et al., 2024a; Li et al., 2025) complements these training-based approaches by conditioning \mathcal{M}_q on additional signals from \mathcal{M}_p , i.e., last-layer hidden states, making proposals more target-aware.

3. System Model

We present the system model for StarSD, where one M_q serves N target instances $\{M_p^{(i)}\}_{i=1}^N$. The model characterizes system throughput as a function of N and the per-request workload by capturing the expected accepted tokens and the iteration time under different load conditions.

3.1. Iteration Definitions

System iterations are indexed by $\gamma = \{1, \dots, \gamma_{\text{end}}\}$, where each iteration corresponds to one draft-side scheduling round, and γ_{end} denotes the total number of scheduling rounds executed during a decoding session. In the γ -th iteration, the draft instance M_q processes one speculative request for each active target instance $M_p^{(i)}$ in a work-conserving order. For a given request, M_q generates a speculative draft with depth d , which is verified by the corresponding $M_p^{(i)}$, and the verification result is returned to M_q before the next iteration. The draft depth d upper-bounds the per-iteration progress and determines the amount of work for each $M_p^{(i)}$. This abstraction allows us to analyze system progress and time cost on a per-iteration basis.

3.2. Per-iteration Acceptance Length

We first quantify the per-iteration progress made by all target instances in one iteration, measured by the number of tokens accepted by $\{M_p^{(i)}\}_{i=1}^N$.

Acceptance probability. We start from a token-level acceptance notion that captures the agreement between \mathcal{M}_q and \mathcal{M}_p . We consider that all target instances $\{M_p^{(i)}\}_{i=1}^N$ are instantiated from the same target model type \mathcal{M}_p , which is common in multi-session serving scenarios, e.g., LLM-based multi-agent systems (Li et al., 2023; Chen et al., 2024a; Wu et al., 2024). The index i distinguishes concurrent decoding sessions that may have different prefixes and thus different next-token distributions. Conditioned on a prefix y , let the next-token distributions of target $M_p^{(i)}$ and draft M_q be $p_i(\cdot | y)$ and $q(\cdot | y)$, respectively. We define the token-level acceptance probability at prefix y as

$$\begin{aligned} \beta_i(y) &\triangleq \sum_x \min\{p_i(x | y), q(x | y)\} \\ &= 1 - D_{\text{LK}}(p_i(\cdot | y), q(\cdot | y)), \end{aligned} \quad (1)$$

where $D_{\text{LK}}(p, q) = \frac{1}{2} \sum_x |p(x) - q(x)|$ denotes the total variation distance between p and q (Leviathan et al., 2023).

This quantity measures how likely a draft proposal from M_q is accepted by $M_p^{(i)}$ under the given prefix y .

Expected accept length. We lift token-level acceptance to an iteration-level quantity by defining the accept length. Let $l_i(d) \in \{0, 1, \dots, d\}$ denote the accept length of $M_p^{(i)}$ in one iteration, i.e., the number of consecutive proposed tokens accepted by $M_p^{(i)}$. This random variable represents the realized per-iteration progress for $M_p^{(i)}$. To obtain the expected accept length, we use a standard tail-sum identity that converts $\mathbb{E}[l_i(d)]$ into a sum of acceptance events.

Lemma 3.1 (Tail-sum identity for bounded accept length). *For any $l_i(d) \in \{0, 1, \dots, d\}$, we have*

$$\mathbb{E}[l_i(d)] = \sum_{j=1}^d \Pr(l_i(d) \geq j). \quad (2)$$

The term $\Pr(l_i(d) \geq j)$ is the probability that the first j proposed tokens are all accepted, and their sum yields the expected accept length.

Proof. Since $l_i(d)$ is non-negative and bounded by d , it can be written as $l_i(d) = \sum_{j=1}^d \mathbf{1}\{l_i(d) \geq j\}$, where $\mathbf{1}\{\cdot\}$ is the indicator function. Taking the expectation on both sides and using the linearity of expectation gives $\mathbb{E}[l_i(d)] = \sum_{j=1}^d \mathbb{E}[\mathbf{1}\{l_i(d) \geq j\}] = \sum_{j=1}^d \Pr(l_i(d) \geq j)$. \square

Closed-form Expression. A common approximation in speculative decoding analysis is that, within one iteration, token acceptances are i.i.d. Bernoulli with an acceptance rate β_i (Leviathan et al., 2023). However, later drafts depend on earlier acceptances in practice, so the independence assumption is an analytical simplification (Chen et al., 2023). Under this approximation

$$\mathbb{E}[l_i(d)] \approx \sum_{j=1}^d \beta_i^j = \frac{\beta_i (1 - \beta_i^d)}{1 - \beta_i}. \quad (3)$$

This expression shows diminishing returns in d when $\beta_i < 1$, as the marginal gain scales with β_i^{d+1} .

Finally, the expected total accepted tokens across $\{M_p^{(i)}\}_{i=1}^N$ in one iteration is

$$\mathbb{E}[l]_\gamma \triangleq \sum_{i=1}^N \mathbb{E}[l_i(d)] \approx \sum_{i=1}^N \frac{\beta_i (1 - \beta_i^d)}{1 - \beta_i}. \quad (4)$$

This quantity aggregates per-iteration progress and serves as the system progress term when interpreting throughput.

3.3. Per-iteration Time Decomposition

We turn to the *time* component of throughput by characterizing the duration of a single iteration under concurrent service. In each iteration, M_q serves N depth- d requests, one from each active target instance $M_p^{(i)}$. The service time for a single depth- d request is

$$S(d) \triangleq d t_s, \quad (5)$$

where t_s is the time for M_q to generate one layer of draft tokens, which remains nearly constant due to parallel execution within a modern accelerator.

After M_q finishes serving a given $M_p^{(i)}$, the earliest time that M_q can receive the next request from the same $M_p^{(i)}$ is determined by the return time as

$$Z(d) \triangleq t_c + t_v, \quad (6)$$

where t_c is the communication time in one iteration and t_v is the time taken for $M_p^{(i)}$ to verify the received draft tokens.

We consider M_q is work-conserving, whenever the request buffer is non-empty, M_q continuously serves pending requests according to a policy such as first-in-first-out. Each target instance $M_p^{(i)}$ issues a new request only after completing verification of its previous one. Under these settings, system load is fully determined by the number of concurrent target instances, without additional effects from scheduling or request reordering.

We next characterize the condition under which the draft instance M_q remains continuously busy in StarSD pipeline.

Lemma 3.2 (A sufficient non-idling condition for M_q). *If*

$$Z(d) \leq (N - 1) S(d), \quad (7)$$

then a work-conserving M_q does not idle due to waiting for verification results from any target instance $M_p^{(i)}$.

Proof. After M_q completes serving a request from some target instance $M_p^{(i)}$, the earliest time at which $M_p^{(i)}$ can issue its next request is $Z(d)$. During this interval, M_q can serve at most one pending request from each of the remaining $N - 1$ target instances, incurring a total service time of $(N - 1)S(d)$. \square

3.4. Per-iteration Throughput

As shown in Fig. 1, we consider two cases depending on whether (7) holds.

Fully-loaded case. When (7) holds, the return time $Z(d)$ of any active $M_p^{(i)}$ can be covered by the M_q -side service spent on the other $N - 1$ active $M_p^{(i)}$. As a result, once the request buffer is populated, M_q can continuously serve

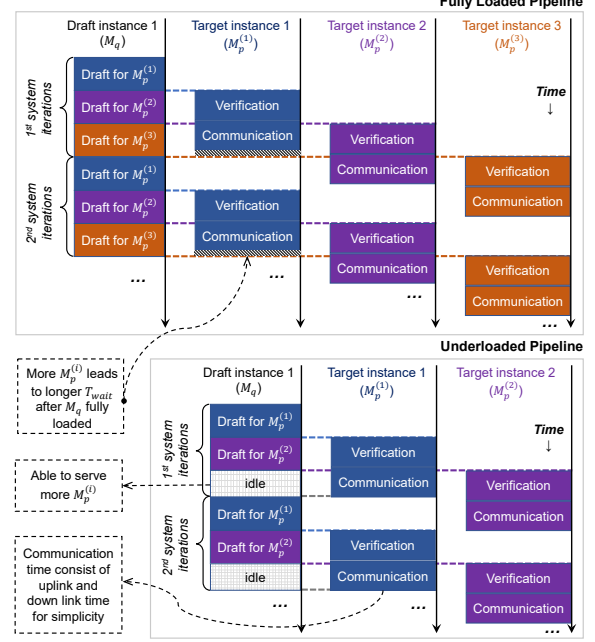


Figure 1. Execution cases of StarSD under different load conditions. **Fully-loaded case** where verification and communication delays of each $M_p^{(i)}$ are overlapped, keeping M_q work-conserving with no idle gaps. **Under-loaded case** where the draft server idles while waiting for a target to return the next request.

requests without observable idle gaps. In this case, the per-iteration time is

$$T_{\gamma\text{full}} = N S(d), \quad (8)$$

since one iteration corresponds to serving N depth- d requests (one per active $M_p^{(i)}$), each taking $S(d)$ time on M_q .

Under-loaded case.

When (7) does not hold, serving the other $N - 1$ active $M_p^{(i)}$ for a total of $(N - 1)S(d)$ time may still be insufficient for the original $M_p^{(i)}$ to complete its return within $Z(d)$. In this case, M_q can become idle due to a temporary lack of pending requests. We quantify this additional waiting time by defining the idle gap per iteration

$$T_{\text{idle}} \triangleq \max\{0, Z(d) - (N - 1)S(d)\}. \quad (9)$$

Thus, the general per-iteration time can be expressed as

$$T_{\gamma} = N S(d) + T_{\text{idle}}. \quad (10)$$

Finally, we define the throughput in the γ -th iteration as

$$O_{\gamma} \triangleq \frac{\mathbb{E}[l]_{\gamma}}{T_{\gamma}}. \quad (11)$$

This definition decouples the expected progress $\mathbb{E}[l]_{\gamma}$ from the time cost T_{γ} , making clear whether throughput is limited by acceptance or by the iteration time overheads. It also enables case-wise interpretation through (8) and (10).

Algorithm 1 StarSD One-for-Many Serving Runtime

```

Input:  $M_q, \{M_p^{(i)}\}_{i=1}^N$ , Prefix  $\hat{y}$ .
Preparation:
    • Handshake: assign each target a unique tag and establish a dedicated port.
    •  $\mathcal{C}[\text{tag}]$ : per-session KV cache for tag.
    •  $\mathcal{Q}_{in}$ : global request buffer ( $\text{tag}, \hat{y}$ ).
    •  $\mathcal{Q}_{out}$ : outgoing queue of replies ( $\text{tag}, \hat{y}$ ).

1: ## In machine hosting  $M_p^{(i)}$ 
2: if  $\text{recv } \hat{y}$  from  $M_q$  then
3:    $y \leftarrow M_p^{(i)}(\hat{y})$  // refer to Algorithm 2 for verification details
4:   send  $y$  to  $M_q$  on the port identified by tag
5: end if
6:
7: ## In machine hosting  $M_q$ 
8: // Receiver
9: while true do
10:    $(\text{tag}, y) \leftarrow \text{recv}$  from any  $M_p^{(i)}$ 
11:   push  $(\text{tag}, y)$  to  $\mathcal{Q}_{in}$ 
12: end while
13: // Draft inference
14: if  $\mathcal{Q}_{in}$  is non-empty then
15:    $(\text{tag}, y) \leftarrow \text{pop } \mathcal{Q}_{in}$ 
16:    $(\hat{y}, \mathcal{C}[\text{tag}]) \leftarrow M_q(y; \mathcal{C}[\text{tag}])$  // refer to Algorithm 2 for inference details
17:   push  $(\text{tag}, \hat{y})$  to  $\mathcal{Q}_{out}$ 
18: end if
19: // Sender
20: if  $\mathcal{Q}_{out}$  not empty then
21:    $(\text{tag}, \hat{y}) \leftarrow \text{pop } \mathcal{Q}_{out}$ 
22:   send  $\hat{y}$  back to  $M_p^{(i)}$  on the port identified by tag
23: end if

```

4. StarSD Implication

This section translates the analytical conditions into StarSD implication principles and examines how throughput scales as the number of target instances increases.

4.1. StarSD Design

We design StarSD by considering the following runtime properties.

Work-conserving draft execution. To match (8)-(10) under asynchronous returns, M_q maintains a global request buffer \mathcal{Q}_{in} , an outgoing buffer \mathcal{Q}_{out} , and runs a non-blocking loop that always serves any pending request, making uncovered return time appear as T_{idle} in (9).

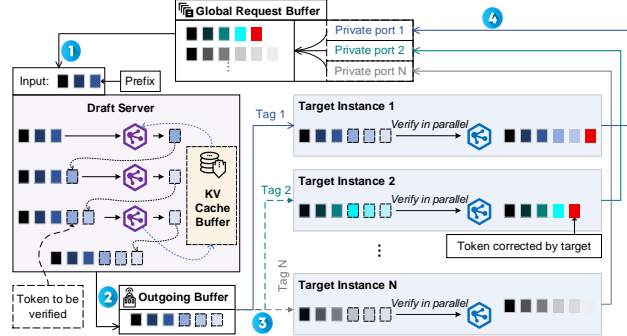


Figure 2. StarSD Pipeline. Use the global request buffer and outgoing buffer to guarantee the work continuity of the draft model.

Per-target state isolation. To preserve the correctness of (1) and (2) under concurrency, StarSD isolates all per-target state, including KV cache and metadata, across target instances by tag via $\mathcal{C}[\text{tag}]$.

Independent return paths. To preserve the return-time decomposition $Z(d) = t_c + t_v$ in (6), we assign each target a unique tag and a dedicated port during a one-time handshake, and reuse these ports for steady-state payload transfer in Algorithm 1.

Algorithm 1 provides one concrete realization of these properties, and Fig. 2 summarizes the resulting execution pipeline. Verified prefixes from multiple target instances are collected into a shared request buffer and served by the draft instance in a work-conserving manner. Drafted tokens are routed back to their corresponding targets for parallel verification, and the verified prefixes re-enter the pipeline for subsequent iterations. By decoupling request arrival, draft execution, and verification returns, this pipeline avoids cross-target head-of-line blocking and enables continuous draft-side execution under concurrent service.

4.2. Insights

While StarSD enables one-for-many serving, its throughput exhibits a trade-off. Figure 3 shows a two-stage behavior as the number of active target instances grows.

Stage I: Under-loaded. When N is small, M_q is under-loaded, the global request buffer is frequently empty, so M_q exhibits idle gaps, and adding more active $M_p^{(i)}$ primarily improves utilization. In this regime, the per- $M_p^{(i)}$ throughput $O_{\gamma}^{(i)}$ stays approximately constant, while the system throughput O_{γ} increases with N because the uncovered return time is gradually amortized across more concurrent requests. This corresponds to the violation of (7), where the uncovered return time appears as T_{idle} in (9), and thus T_{γ} follows (10).

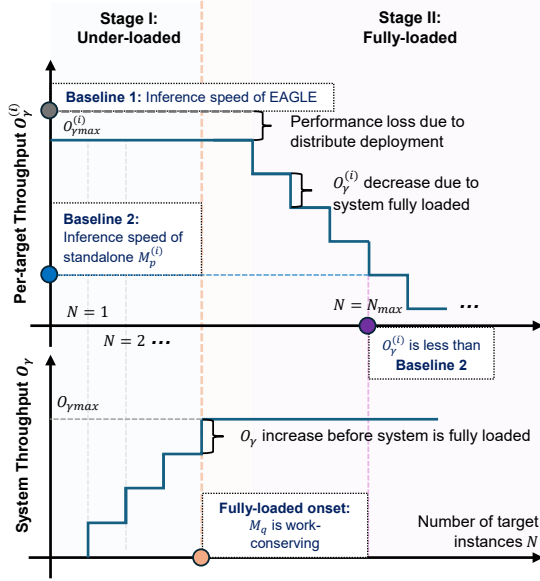


Figure 3. StarSD framework behavior when scaling the number of target instances. Baseline 1 stands for the throughput of SOTA speculative decoding that is deployed on a single accelerator. Baseline 2 is the standalone inference speed of an LLM.

Stage II: Fully-loaded. As N increases, the idle gap vanishes, the global request buffer becomes persistently non-empty, and M_q turns work-conserving. Beyond this point, increasing N no longer increases the service capacity of M_q but introduces queueing in the global request buffer. Consequently, the waiting time before a request is served increases T_γ , which reduces the per- $M_p^{(i)}$ throughput $O_\gamma^{(i)}$, while O_γ saturates near its maximum. Formally, the full-load onset is the smallest N such that (7) holds. Equivalently, for

$$N \geq N_{\text{full}} \triangleq \left\lceil \frac{Z(d)}{S(d)} \right\rceil + 1, \quad (12)$$

we have $T_{\text{idle}} = 0$ and T_γ follows (8).

Importantly, admitting more $M_p^{(i)}$ can still be beneficial after full load as long as the resulting $O_\gamma^{(i)}$ remains above the throughput of a standalone $M_p^{(i)}$. We denote by N_{max} the largest active set size such that $O_\gamma^{(i)}$ does not fall below this point. Beyond N_{max} , additional concurrency degrades per- $M_p^{(i)}$ throughput below what $M_p^{(i)}$ can achieve without M_q . This observation motivates a practical admission rule at M_q , reject new $M_p^{(i)}$ requests when $N > N_{\text{max}}$ to preserve per- $M_p^{(i)}$ throughput higher than the standalone inference speed of $M_p^{(i)}$.

Packing advantage in practice. Beyond throughput, StarSD improves practical memory packing on accelerators. Colocating one target instance with its draft model forms fixed pairs that occupy large, indivisible memory

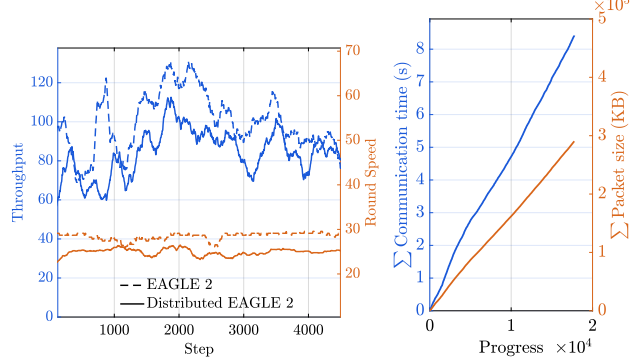


Figure 4. Throughput loss due to distribute deployment of EAGLE and communication overhead.

blocks. Under a fixed accelerator memory budget, such coarse-grained pairing limits how many target instances can be placed concurrently and leaves fragmented memory regions. By decoupling drafting from verification and providing the draft model as a shared service, StarSD’s finer-grained placement allows accelerator memory to be primarily filled with target instances, increasing target density and enabling either more concurrent replicas or longer context lengths under the same hardware budget.

5. Experiments

We evaluate StarSD along three dimensions, i.e., its distributed execution characteristics, its scalability under one-for-many concurrency, and its practical draft-side performance behavior under different runtime regimes.

5.1. Distributed Behavior of StarSD

Since StarSD does not modify model weights or the speculative decoding algorithm, performance differences arise solely from system effects, namely communication overhead introduced by distribution and potential gains from parallel execution. Thus, we evaluate StarSD on the full MT-Bench benchmark (Zheng et al., 2023) using EAGLE 2 (Li et al., 2024b) as a representative backend. To isolate the cost of distribution, we consider the $N = 1$ case, where the draft instance M_q and the target instance M_p are placed on different accelerators. In this configuration, StarSD reduces to a distributed deployment of EAGLE 2, enabling a direct measurement of cross-device communication overhead.

As shown in Fig. 4(a), we report throughput from two perspectives, (1) system throughput O_γ , which fluctuates noticeably across MT-Bench due to prompt-dependent acceptance lengths, and (2) the round speed R_q of M_q which is proportional to O_γ and prove in C.1, it provides a smoother perspective to observe performance. To reflect the cost

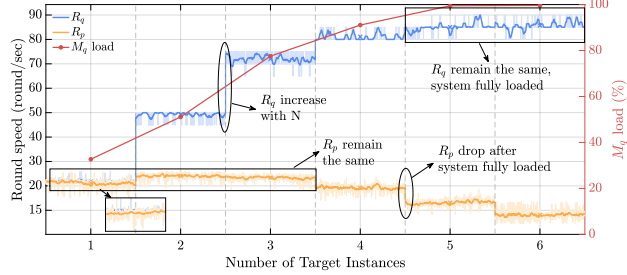


Figure 5. Round speed R_q and R_p , load of M_q under varying numbers of target instances N .

Table 1. System performance metrics as the number of target instances N increases.

Metric	EAGLE	StarSD with different numbers of target instances N					
		1	2	3	4	5	6
Throughput (tokens/s)							
O_γ	94.3	79.9	167.6	246.3	266.6	285.5	288.7
$O_\gamma^{(i)}$	118.5	86.6	100.9	98.3	80.94	69.49.	57.78
Time breakdown (ms)							
t_s	1.78	2.24	1.36	1.36	1.42	1.46	1.46
T_{wait}	—	0.01	0.50	0.60	3.90	13.0	22.3
T_{idle}	—	30.6	9.8	3.4	0.6	0.0	0.0
Round speed (round/s)							
R_q	26.8	20.90	49.25	72.26	81.54	85.52	85.84
R_p	26.8	20.90	24.07	23.38	19.73	16.64	14.10
Utilization (%)							
M_q load	—	33.3	50.3	75.4	91.4	99.5	99.6

of distributed deployment, we measure end-to-end serving performance in the deployed setting, so the experiment results naturally include cross-device overheads such as communication latency shown in Fig. 4(b), message serialization and deserialization, and GPU-CPU memory transfers. Our implementation is deployment-agnostic and supports multi-accelerator execution either within a single machine or across machines. Accordingly, we use socket-based communication rather than hardware-specific backends, e.g., NVLink, trading some performance for portability. This observation aligns with recent findings in distributed LLM serving that cross-accelerator data movement can incur non-trivial overhead and lead to a measurable performance drop under equivalent accelerator resources (Li et al., 2025).

5.2. Scaling Behavior of StarSD

To evaluate one-for-many scaling, we vary the number of concurrent target instances N served by a single draft instance M_q and examine how system performance evolves with increasing concurrency. Fig. 5 reports the round speeds R_q and R_p under different N . As N increases from 1 to 3, R_q grows substantially, while R_p changes only modestly. This behavior matches the *under-loaded* regime in Section 4.2, where serving additional targets reduces draft-side idle gaps by overlapping verification and communica-

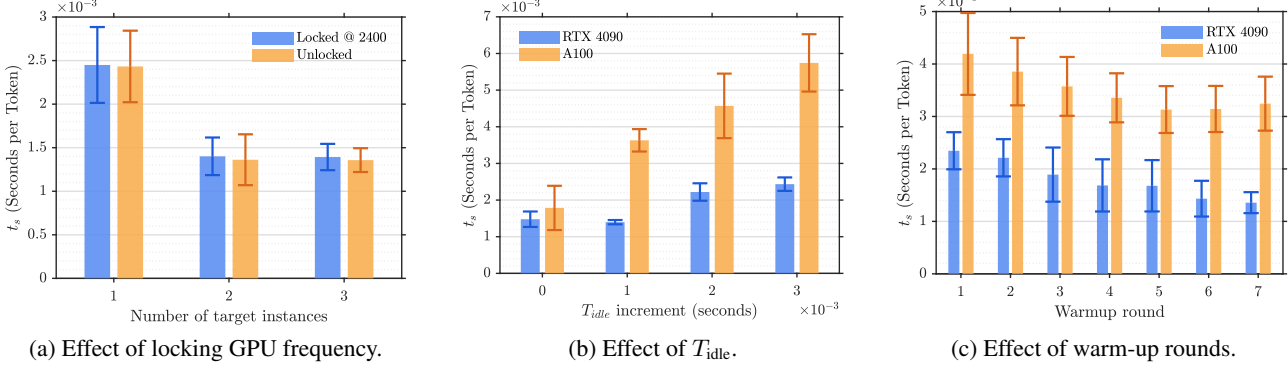
tion latency across requests. At $N = 4$, R_q approaches its maximum, indicating that M_q is close to full utilization and the system begins to enter the *fully-loaded* regime described in Section 4.2. Further increasing N provides only marginal improvement in R_q , while R_p decreases noticeably due to queueing delays before requests are processed by M_q .

To demonstrate the universality of StarSD, we evaluate both intra-node and inter-node configurations as detailed in Appendix H, and summarize system performance for up to six target instances in Table 1. In the intra-node setting, multiple target instances run on distinct GPUs within a single server, while in the inter-node setting, target instances are distributed across multiple servers connected by a local-area network. Specifically, our deployment uses seven GPUs across two servers. One server hosts four RTX 4090 GPUs, running a draft model M_q and three target instances, while the other server hosts three A100 GPUs, each running one target instance. As N increases, targets are first activated on the RTX 4090 server, and targets on the A100 server are used when $N > 3$. The shared M_q server serves all active targets across both machines. All metrics are measured end-to-end and therefore include communication latency and cross-machine serialization overhead, showing that StarSD remains portable and effective across both single-server and multi-server deployments. Beyond throughput and round speed, we report two delay metrics, i.e., the draft-side idle time T_{idle} , which captures how long M_q remains idle between requests, and the queueing wait time T_{wait} , which measures how long a request waits in the global buffer before service. These metrics explain a counter-intuitive trend in Table 1, i.e., when $N = 1$, R_p is lower than at $N = 2$, consistent with a large T_{idle} . Empirically, excessive idle gaps push M_q into an unfavorable operating regime and degrade its per-token inference speed.

5.3. Execution Regimes and Performance Dynamics

As suggested by the results in Table 1, a major source of StarSD’s system-level performance gain comes from eliminating cold-start and idle gaps on the draft side. To further analyze this effect and verify that the observed variation in the inference speed of M_q is not specific to a particular accelerator, we conduct controlled experiments by forming a single draft-target pair and evaluating it independently on an RTX 4090 GPU and on an A100 GPU.

We first rule out GPU frequency scaling as a confounding factor by instrumenting the graphics clock before each inference. As shown in Fig. 6(a), the same slowdown trend appears under both the default Dynamic Voltage and Frequency Scaling (DVFS) policy and a fixed clock of 2400 MHz, indicating that frequency changes are not the cause. To precisely control idle behavior, we then inject artificial delays on the draft side by pausing M_q for a prescribed du-



(a) Effect of locking GPU frequency.

(b) Effect of T_{idle} .

(c) Effect of warm-up rounds.

Figure 6. Per-token generation time analysis of M_q under warm-up at $T_{idle} = 0.03$ s, GPU frequency control, and T_{idle} variation.

ration after receiving each request, thereby inducing a target T_{idle} . Figure 6(b) shows that per-token inference time remains stable when T_{idle} is either small or large, but degrades in an intermediate regime where increasing T_{idle} leads to a monotonic slowdown and higher run-to-run variance. Together, these results indicate that sustained, continuous execution keeps the draft model in a favorable operating state, while intermittent idle gaps introduce transient inefficiencies that increase both latency and variability.

We further examine the warm-up effect shown in Fig. 6(c) by inserting additional draft-side executions after an idle gap and before normal generation begins. In this setup, M_q generates a small number of warm-up tokens to transition back toward a steady execution state. As the number of warm-up rounds increases, the per-token inference speed improves and then stabilizes, with diminishing gains beyond a modest threshold. At low warm-up counts, the execution behavior is comparable to the $N = 1$ setting in Table 1, which exhibits an idle gap of approximately $T_{idle} \approx 0.03$ second and degraded performance. As warm-up rounds increase, the effective idle impact is reduced to about 0.014 second, leading to faster and more stable inference.

6. Related Work

Speculative Decoding. Speculative decoding accelerates autoregressive generation by having a lightweight draft propose tokens and a stronger target verify them while preserving the target distribution (Leviathan et al., 2023; Chen et al., 2023). Follow-up work improves efficiency by proposing and verifying multiple candidates per iteration. Tree-based speculative inference verifies a token tree in parallel to better exploit GPU parallelism (Miao et al., 2024; Chen et al., 2024b; Wang et al., 2025), and other variants expand proposals via multi-branch or multi-head drafting under exact acceptance rules (Cai et al., 2024).

LLM Serving Under Memory Pressure. LLM serving is often bottlenecked by the KV-cache footprint, which limits

batch size and makes co-locating an additional draft model challenging. vLLM reduces KV-cache fragmentation via paging-style management (Kwon et al., 2023). Beyond single-GPU settings, systems disaggregate prefill and decode to reduce interference and improve goodput (Zhong et al., 2024), and phase-splitting designs similarly separate prompt and token phases across machines (Patel et al., 2024). These results suggest that, under realistic batch sizes and KV-cache pressure, hosting both a large target and a draft on one accelerator can be impractical.

Distributed and Networked Speculative Decoding.

Placing draft and target on different accelerators turns speculative decoding into a distributed pipeline where communication and asynchronous returns shape utilization. Prior work explores edge settings, e.g., lightweight edge drafts with server-side verification (Li et al., 2025), and distributed speculative inference that leverages multiple drafters, targets and task parallelism (Timor et al., 2024; Venkatesha et al., 2025; Gao et al., 2025). SpecEdge further splits inference between edge and server GPUs via speculative decoding and pipeline-aware scheduling, exchanging only token outputs over the network (Park et al., 2025). Overall, once drafting and verification are disaggregated, performance depends not only on acceptance behavior but also on communication efficiency and scheduling.

7. Conclusion

StarSD is a one-for-many speculative decoding framework that allows a single draft model to efficiently serve multiple target instances. By keeping the draft side work-conserving under asynchronous verification, StarSD eliminates idle gaps that limit the efficiency in distributed deployments. Experiments across heterogeneous settings show that this design improves utilization and throughput without modifying model weights or generation semantics, making speculative decoding more practical under realistic memory and deployment constraints.

Impact Statement

StarSD enables one-for-many speculative decoding by decoupling drafting and verification across distributed accelerators, allowing a single draft model to serve multiple target instances in a work-conserving manner. This can improve utilization and reduce deployment overheads under memory and resource constraints, supporting more flexible allocation across heterogeneous devices in both cluster and edge serving environments. However, StarSD may also introduce risks. By lowering the cost of LLM inference, it can make large-scale misuse easier. More importantly, the shared draft model can become a concentrated trust point, it may transiently hold multiple sessions' prompts, intermediate prefixes, and cached decoding state across served targets. If the draft service is compromised, an attacker could potentially access sensitive user inputs or session traces, leading to severe privacy leakage. To mitigate these risks, deployments should treat the draft service as a high-sensitivity component. Enforce strong isolation between sessions, minimize and protect in-memory and on-disk artifacts including KV caches and logs, use authenticated and encrypted channels for inter-node communication, and apply access control, rate limiting, and auditing to detect abuse and intrusion.

References

Cai, T., Li, Y., Geng, Z., Peng, H., Lee, J. D., Chen, D., and Dao, T. Medusa: Simple LLM inference acceleration framework with multiple decoding heads. *arXiv preprint arXiv:2401.10774*, 2024.

Chen, C., Borgeaud, S., Irving, G., Lespiau, J.-B., Sifre, L., and Jumper, J. Accelerating large language model decoding with speculative sampling. *arXiv preprint arXiv:2302.01318*, 2023.

Chen, W., Su, Y., Zuo, J., Yang, C., Yuan, C., Chan, C.-M., Yu, H., Lu, Y., Hung, Y.-H., Qian, C., et al. Agentverse: Facilitating multi-agent collaboration and exploring emergent behaviors. In *International Conference on Learning Representations*, 2024a.

Chen, Z., May, A., Svirschevski, R., Huang, Y., Ryabinin, M., Jia, Z., and Chen, B. Sequoia: Scalable and robust speculative decoding. In Globerson, A., Mackey, L., Belgrave, D., Fan, A., Paquet, U., Tomczak, J., and Zhang, C. (eds.), *Advances in Neural Information Processing Systems*, volume 37, pp. 129531–129563. Curran Associates, Inc., 2024b.

Gao, L., Liu, J., Xu, H., Zhang, X., Liao, Y., and Huang, L. Collaborative speculative inference for efficient LLM inference serving. *arXiv e-prints*, art. arXiv:2503.10325, March 2025.

Hu, Y., Guo, J., Feng, X., and Zhao, T. Adaspec: Selective knowledge distillation for efficient speculative decoders. *arXiv preprint arXiv:2510.19779*, 2025.

Kwon, W., Li, Z., Zhuang, S., Sheng, Y., Zheng, L., Yu, C. H., Gonzalez, J., Zhang, H., and Stoica, I. Efficient memory management for large language model serving with pagedattention. In *Proceedings of the 29th symposium on operating systems principles*, pp. 611–626, 2023.

Leviathan, Y., Kalman, M., and Matias, Y. Fast inference from transformers via speculative decoding. In Krause, A., Brunskill, E., Cho, K., Engelhardt, B., Sabato, S., and Scarlett, J. (eds.), *Proceedings of the 40th International Conference on Machine Learning*, volume 202 of *Proceedings of Machine Learning Research*, pp. 19274–19286, 23–29 Jul 2023.

Li, G., Hammoud, H., Itani, H., Khizbulin, D., and Ghanem, B. Camel: Communicative agents for "mind" exploration of large language model society. In Oh, A., Naumann, T., Globerson, A., Saenko, K., Hardt, M., and Levine, S. (eds.), *Advances in Neural Information Processing Systems*, volume 36, pp. 51991–52008. Curran Associates, Inc., 2023.

Li, J., Zhu, Y., Lee, E. K., and Nahrstedt, K. Revisiting disaggregated large language model serving for performance and energy implications. *arXiv e-prints*, art. arXiv:2601.08833, November 2025.

Li, X., Spatharakis, D., Ghafouri, S., Fan, J., Vandieren-donck, H., John, D., Ji, B., and Nikolopoulos, D. S. Sled: A speculative LLM decoding framework for efficient edge serving. In *Proceedings of the Tenth ACM/IEEE Symposium on Edge Computing*, pp. 1–8, 2025.

Li, Y., Wei, F., Zhang, C., and Zhang, H. Eagle: Speculative sampling requires rethinking feature uncertainty. *arXiv preprint arXiv:2401.15077*, 2024a.

Li, Y., Wei, F., Zhang, C., and Zhang, H. Eagle-2: Faster inference of language models with dynamic draft trees. *arXiv preprint arXiv:2406.16858*, 2024b.

Li, Y., Wei, F., Zhang, C., and Zhang, H. Eagle-3: Scaling up inference acceleration of large language models via training-time test. *arXiv e-prints*, art. arXiv:2503.01840, March 2025.

Liu, X., Hu, L., Bailis, P., Cheung, A., Deng, Z., Stoica, I., and Zhang, H. Online speculative decoding. *arXiv preprint arXiv:2310.07177*, 2023.

Miao, X., Oliaro, G., Zhang, Z., Cheng, X., Wang, Z., Zhang, Z., Wong, R. Y. Y., Zhu, A., Yang, L., Shi, X.,

et al. Specinfer: Accelerating large language model serving with tree-based speculative inference and verification. In *Proceedings of the 29th ACM International Conference on Architectural Support for Programming Languages and Operating Systems, Volume 3*, pp. 932–949, 2024.

Park, J., Cho, S., and Han, D. Specedge: Scalable edge-assisted serving framework for interactive LLMs. *arXiv preprint arXiv:2505.17052*, 2025.

Patel, P., Choukse, E., Zhang, C., Shah, A., Goiri, I., Maleki, S., and Bianchini, R. Splitwise: Efficient generative LLM inference using phase splitting. In *2024 ACM/IEEE 51st Annual International Symposium on Computer Architecture*, pp. 118–132. IEEE, 2024.

Sheng, Y., Zheng, L., Yuan, B., Li, Z., Ryabinin, M., Chen, B., Liang, P., Ré, C., Stoica, I., and Zhang, C. Flexgen: High-throughput generative inference of large language models with a single GPU. In *International Conference on Machine Learning*, pp. 31094–31116. PMLR, 2023.

Timor, N., Mamou, J., Korat, D., Berchansky, M., Pereg, O., Wasserblat, M., Galanti, T., Gordon, M., and Harel, D. Distributed speculative inference (DSI): Speculation parallelism for provably faster lossless language model inference. *arXiv preprint arXiv:2405.14105*, 2024.

Venkatesha, Y., Kundu, S., and Panda, P. Fast and cost-effective speculative edge-cloud decoding with early exits. *arXiv e-prints*, art. arXiv:2505.21594, May 2025.

Wang, J., Su, Y., Li, J., Xia, Q., Ye, Z., Duan, X., Wang, Z., and Zhang, M. Opt-tree: Speculative decoding with adaptive draft tree structure. *Transactions of the Association for Computational Linguistics*, 13:188–199, 02 2025. ISSN 2307-387X.

Wu, Q., Bansal, G., Zhang, J., Wu, Y., Li, B., Zhu, E., Jiang, L., Zhang, X., Zhang, S., Liu, J., et al. Autogen: Enabling next-gen LLM applications via multi-agent conversations. In *First Conference on Language Modeling*, 2024.

Zheng, L., Chiang, W.-L., Sheng, Y., Zhuang, S., Wu, Z., Zhuang, Y., Lin, Z., Li, Z., Li, D., Xing, E., et al. Judging LLM-as-a-judge with mt-bench and chatbot arena. *Advances in neural information processing systems*, 36: 46595–46623, 2023.

Zhong, Y., Liu, S., Chen, J., Hu, J., Zhu, Y., Liu, X., Jin, X., and Zhang, H. Distserve: Disaggregating prefill and decoding for goodput-optimized large language model serving. In *18th USENIX Symposium on Operating Systems Design and Implementation*, pp. 193–210, 2024.

Zhou, Y., Lyu, K., Rawat, A. S., Menon, A. K., Ros-tamizadeh, A., Kumar, S., Kagy, J.-F., and Agarwal, R. Distillspec: Improving speculative decoding via knowledge distillation. *arXiv preprint arXiv:2310.08461*, 2023.

A. Overview of Supplementary Material

This appendix provides supplementary algorithmic descriptions, deployment illustrations, and experimental artifacts that support the results in the main text. For reproducibility, command-line snippets and representative log excerpts are highlighted in `typewriter` font. The appendix is organized as follows:

1. **Motivation of StarSD:** We motivate StarSD from practical deployment constraints and the resulting inefficiencies of distributed speculative decoding, explaining why a one-for-many draft service is desirable in Section [B](#).
2. **Mathematical Justification:** We provide further mathematical Justification in Section [C](#).
3. **Algorithm Details:** We describe the EAGLE-based speculative decoding procedure used in StarSD, including the key steps of proposal, verification, and correction, in Section [D](#).
4. **Implementation Details:** We present system-level implementation details of StarSD, including the one-time connection establishment protocol, the steady-state request execution loop, the decoupled communication that computes runtime at the draft server, and tag-indexed per-session state management, e.g., KV cache lifecycle and speculative metadata in Section [E](#).
5. **Extended GPU Experiment Details:** We provide additional reproducibility artifacts for the GPU frequency-control study and draft-side inference-time measurements in Sections [F](#) and [G](#).
6. **Deployment Illustrations:** We summarize representative deployment topologies and illustrate the end-to-end distributed pipeline in Section [H](#).
7. **Discussion and Future Directions:** We discuss limitations of the current design and outline future directions in Section [I](#).

B. Motivation

Recent advances in speculative decoding have largely focused on improving the draft model by better aligning its token distribution with the target model. However, most existing frameworks implicitly assume that the draft instance M_q and the target instance M_p can be co-located on a single accelerator, e.g., a GPU. In practical deployments, this assumption often does not hold. Many real systems operate under heterogeneous and resource-constrained settings, including edge clusters and mid-scale cloud servers, where accelerator memory is limited and shared by multiple services. The weights may barely fit, but the remaining memory must still accommodate KV cache and runtime buffers. In practice, this sharply reduces the KV cache budget, hence affect the context length, which is especially problematic in multi-tenant deployments where one GPU also serves other inference tasks. Even with compression or quantization, co-locating M_q and M_p can remain impractical or introduce nontrivial accuracy, engineering, and operational costs.

A natural response is to disaggregate the deployed instances M_q and M_p across different accelerators, e.g., GPU. Distributed speculative decoding has been explored in prior work, but most existing designs do not address a core inefficiency inherent to the draft-then-verify workflow. When the target instance M_p is verifying draft tokens, the accelerator hosting the draft instance M_q is idle; when M_q is drafting, the M_p accelerator is underutilized. This alternating execution pattern reduces effective hardware utilization and makes M_q execution bursty, with short compute phases separated by idle gaps induced by verification latency and inter-accelerator communication. These idle gaps have system-level consequences that are also largely overlooked in prior work. Even when the decoding depth is unchanged, bursty execution prevents M_q from sustaining a stable high-throughput execution state and may trigger repeated per-iteration transients (e.g., kernel reactivation and cache coldness), leading to increased draft-step latency and higher variance across decoding iterations.

More fundamentally, the generated output is ultimately dictated by the target instance M_p , while M_q serves as auxiliary compute overhead. From a system perspective, this overhead should be amortized across multiple target instances rather than dedicated to a single M_p . These observations motivate a one-for-many design in which a single M_q multiplexes requests from multiple $M_p^{(i)}$. Such a design allows verification responses to arrive more continuously, reduces idle gaps on the draft accelerator, and improves system-level utilization.

C. Mathematical Justification

C.1. Metric Justification of Draft and Verify Round Speed

We consider a fixed dataset \mathcal{D} , a fixed decoding configuration, and a fixed model pair (M_p, M_q) with depth d . Across deployments, we keep the model weights and the decoding algorithm unchanged. Hence, for any prefix y encountered during decoding on \mathcal{D} , the next-token distributions $p(\cdot | y)$ and $q(\cdot | y)$ are invariant up to numerical nondeterminism, and the induced acceptance behavior is invariant in expectation. Under the standard approximation, the expected accepted length per draft proposal

$$\bar{\ell} \triangleq \mathbb{E}[l(d)], \quad (\text{C.1})$$

is deployment-invariant.

Round speeds. Let R_q denote the rate per unit time at which the draft model executes the token-generation routine that produces a depth- d proposal, each such execution yields an accepted length $l(d)$ in the subsequent verification step. Let R_p denote the rate per unit time at which a target instance executes a verification routine. Both R_q and R_p are measured in the steady state.

Throughput as tokens per unit time. Recall that the system throughput (11) from the draft-side view is

$$O_\gamma \triangleq \frac{\mathbb{E}[l]_\gamma}{T_\gamma}, \quad (\text{C.2})$$

where $\mathbb{E}[l]_\gamma$ is the expected number of accepted tokens contributed in an interval of duration T_γ . From the target-side view, we similarly define the per-target throughput for instance i as

$$O_\gamma^{(i)} \triangleq \frac{\mathbb{E}[l]_\gamma^{(i)}}{T_\gamma}. \quad (\text{C.3})$$

Positive correlation with R_q . Over any time window of length T_γ , the number of draft-generation executions is approximately $R_q T_\gamma$ in expectation. Each execution contributes an accepted length with expectation $\bar{\ell}$. Therefore,

$$\mathbb{E}[l]_\gamma \approx (R_q T_\gamma) \bar{\ell}, \quad O_\gamma = \frac{\mathbb{E}[l]_\gamma}{T_\gamma} \approx \bar{\ell} R_q. \quad (\text{C.4})$$

Since $\bar{\ell} > 0$ under fixed \mathcal{D} and decoding setup, O_γ is monotone increasing in R_q , i.e., R_q is positively correlated with O_γ .

Positive correlation with R_p . Fix a target instance $M_p^{(i)}$. Over a window of length T_γ , the expected number of verification executions by this instance is approximately $R_p T_\gamma$. Each verification round finalizes one proposal and advances the decoded sequence by an accepted length with expectation $\bar{\ell}$. Thus,

$$\mathbb{E}[l]_\gamma^{(i)} \approx (R_p T_\gamma) \bar{\ell}, \quad O_\gamma^{(i)} = \frac{\mathbb{E}[l]_\gamma^{(i)}}{T_\gamma} \approx \bar{\ell} R_p, \quad (\text{C.5})$$

which implies that $O_\gamma^{(i)}$ is monotone increasing in R_p and hence R_p is positively correlated with the throughput of the i -th target instance.

Bottleneck regime. In practice, draft and verification must be matched, so the realized throughput is governed by the slower side. This is consistent with the upper-bound intuition

$$O_\gamma \lesssim \bar{\ell} \min\{R_q, R_p\}, \quad (\text{C.6})$$

and increasing either R_q or R_p cannot decrease throughput.

Special case: 1-for-1 in StarSD. When there is only one target instance, i.e., $N = 1$, the system has a single verification stream, so the per-target throughput coincides with the system throughput

$$O_\gamma^{(i)} = O_\gamma. \quad (\text{C.7})$$

Moreover, the execution forms a tightly coupled loop, where each draft-generation round on M_q produces exactly one proposal, and each proposal triggers exactly one verification round on M_p . Therefore, in steady state, the number of draft rounds and verification rounds are equal over any long horizon, implying

$$R_q = R_p. \quad (\text{C.8})$$

Combining (C.5) and (C.7), both metrics induce the same monotone proxy for throughput in the 1-for-1 setting:

$$O_\gamma = \bar{\ell} R_q = \bar{\ell} R_p. \quad (\text{C.9})$$

D. EAGLE Algorithm Details

Setting and notation. Let y denote the *verified prefix* at the beginning of one speculative iteration. EAGLE uses a draft model M_q to construct a k -ary proposal tree of depth d , and a target model M_p to verify candidate paths. A candidate path is represented as `tree_path` = $[x_1, \dots, x_d]$. During tree expansion, the draft model M_q produces next-token distributions at each depth. We denote the distribution at depth t by $q_t(\cdot)$. The correction step uses the corresponding draft probability $q_{l+1}(x)$ in $\text{norm}(\max(0, p_{l+1}(x) - q_{l+1}(x)))$. During verification, running M_p along the prefixes induced by a path produces target-side distributions $p_1(\cdot), \dots, p_{d+1}(\cdot)$.

Initialization. EAGLE starts each iteration from a verified prefix y . In the first iteration, M_q samples a root token x and an accompanying `hidden_state` from the distribution conditioned on y provided by M_p , in later iterations, it anchors the new proposal tree at the last verified token $y[-1]$.

Tree expansion with caching. The proposal tree is expanded layer-by-layer to depth d with top- k branching. Before expanding each layer, the algorithm initializes the draft KV cache from y or incrementally updates it following the currently selected `target_path`. The expansion routine `EXPAND_LAYER` is executed in parallel over the current tree frontier, and the draft probabilities $q_t(\cdot)$ needed by the correction step are stored in the tree metadata.

Verification and accept-length computation. For each candidate path $\pi = [x_1, \dots, x_d]$, the target model M_p is evaluated on the sequence of induced prefixes $y, y + x_1, \dots, y + [x_1, \dots, x_d]$ to produce $p_1(\cdot), \dots, p_{d+1}(\cdot)$. The algorithm samples r_1, \dots, r_d and gets the accepted length l using the test in Alg. 2.

Correction and best-path selection. If $l < d$, the algorithm forms a corrected distribution $p'(x) \leftarrow \text{norm}(\max(0, p_{l+1}(x) - q_{l+1}(x)))$ and appends one corrected token after the accepted prefix. Otherwise, it keeps the accepted prefix of length l (which equals d in this case). Finally, it selects the path with the largest accepted length and returns $y + \text{target_path}$ along with the updated `hidden_state` of the selected path.

Algorithm 2 EAGLE Speculative Decoding

```

1: Input:  $M_q, M_p$ , verified prefix  $y$ , depth  $d$ , top- $k$   $k$ 
2: Output:  $y + \text{target\_path}$  and updated hidden_state
3: accept_length  $\leftarrow 0$  // best accepted length among all verified paths
4: target_path  $\leftarrow []$  // path selected for this iteration
5:
6: if First Iteration then
7:   // Initialize root token and hidden state to start  $M_q$ 
8:    $x, \text{hidden\_state} \sim p(y)$ 
9:    $\text{tree} \leftarrow x$  // root of the proposal tree
10: else
11:   // Use the last verified token as the tree root
12:    $\text{tree} \leftarrow y[-1]$ 
13: end if
14:
15: // Build a depth- $d$  proposal tree with branching factor  $k$ 
16: for  $t = 1$  to  $d$  do
17:   // KV-cache maintenance for draft expansion (prefix init or incremental update)
18:   if kv_cache is empty then
19:      $\text{kv\_cache} \leftarrow \text{INITKV}(y, \text{hidden\_state})$  // cache corresponds to the verified prefix
20:   else
21:      $\text{kv\_cache} \leftarrow \text{UPDATEKV}(\text{target\_path}, \text{kv\_cache}, \text{hidden\_state})$  // follow the currently selected path
22:   end if
23:   // Expand one tree layer in parallel using  $M_q$  (top- $k$  per node)
24:    $\text{tree} \leftarrow \text{EXPANDLAYER}(\text{tree}, \text{hidden\_state}, M_q, k)$ 
25: end for
26:
27: // Verify candidate paths in parallel
28: for  $n = 1$  to  $k^d$  do
29:    $\text{tree\_path} \leftarrow \text{tree}[n]$ 
30:   // tree_path corresponds to  $\pi = [x_1, \dots, x_d]$ 
31:   // Run  $M_p$  along prefixes induced by the path, can be executed in parallel
32:    $p_1(x), \dots, p_{d+1}(x) \leftarrow M_p(y), \dots, M_p(y + [x_1, \dots, x_d])$ 
33:   // Determine accept length on this path via stochastic test
34:    $r_1 \sim U(0, 1), \dots, r_d \sim U(0, 1)$ 
35:    $l \leftarrow \min(\{i - 1 \mid 1 \leq i \leq d, r_i > p_i(x)\} \cup \{d\})$ 
36:   // Prepare continuation (either accept full prefix, or apply one-step correction)
37:    $p'(x) \leftarrow p_{l+1}(x)$ 
38:   if  $l < d$  then
39:      $p'(x) \leftarrow \text{norm}(\max(0, p_{l+1}(x) - q_{l+1}(x)))$ 
40:      $\text{tree\_path} \leftarrow \text{tree\_path}[:l].\text{append}(t \sim p'(x))$  // accept first  $l$  tokens, then sample one corrected token
41:   else
42:      $\text{tree\_path} \leftarrow \text{tree\_path}[:l]$  // accept the whole depth- $d$  path
43:   end if
44:   // Select the path with the largest accept length
45:   if  $l > \text{accept\_length}$  then
46:      $\text{accept\_length} \leftarrow l$ 
47:      $\text{target\_path} \leftarrow \text{tree\_path}$ 
48:   end if
49: end for
50:
51: return  $y + \text{target\_path}, \text{hidden\_state}$ 

```

E. Implementation Details of StarSD

This appendix provides implementation-level details and covers the following topics.

- One-time connection establishment protocol.
- Steady-state request execution loop and payload handling.
- Decoupling communication from draft inference on M_q using separate logical components or threads.
- Tag-indexed state management, including KV cache lifecycle and other per-session metadata.
- How these details realize the design requirements in Section 5.
- Work-conserving execution to support (8)-(10).
- Per-session isolation to keep $\beta_i(y)$ in (1) and $l_i(d)$ in (2) well-defined.
- Clean time decomposition to preserve $Z(d) = t_c + t_v$ in (6) and $S(d) = dt_s$ in (5).

E.1. Connection Establishment

One-time handshake per $M_p^{(i)}$. Each $M_p^{(i)}$ performs an initial handshake with M_q through a public port. Upon the first request from this $M_p^{(i)}$, M_q allocates (i) a private communication port and (ii) a unique tag. All subsequent messages between this $M_p^{(i)}$ and M_q are sent through the private port, and the tag is attached to every request to identify the corresponding per-session states at M_q . By isolating the control plane, i.e., handshake from the data plane, i.e., per-iteration messages, we ensure t_c in (6) corresponds to the minimal, repeated payload transfer rather than connection management overhead.

E.2. Steady-State Request Execution

Request execution loop. Given a user prompt, $M_p^{(i)}$ begins decoding and produces an initial token. Then, in each iteration, $M_p^{(i)}$ sends the verified prefix or the newly verified token, along with its tag, to M_q via the private port. The payload follows the minimal-transfer design of the distributed EAGLE setting to reduce the per-iteration communication cost. Upon receiving a tagged request, M_q pushes it into the global request buffer. When the M_q inference worker becomes available, it selects a buffered request using a work-conserving scheduling policy (e.g., first-in-first-out). Before inference, M_q retrieves the corresponding KV cache using the tag, executes draft inference, and updates the KV cache upon completion. The draft output is written to the per- $M_p^{(i)}$ communication channel and sent back to $M_p^{(i)}$ via the corresponding private port, where it is verified and used to form the next request.

E.3. Decoupling Communication and Draft Inference on M_q

Separate communication and inference components. As shown in Fig. 2, M_q consists of two logical components: (i) a communication component that receives requests and appends them to the global request buffer, and (ii) an inference component that repeatedly selects and executes buffered requests as long as the buffer is non-empty. Each active $M_p^{(i)}$ is associated with its own private port and a dedicated communication channel at M_q , preventing cross-session interference while keeping M_q work-conserving. This decoupling is required for the service-time model $S(d) = dt_s$ in (5) in which I/O stalls do not backpressure the compute loop, so the measured draft-side service remains dominated by pure compute rather than network latency. In addition, it helps keep the per-iteration transfer cost accounted for in $Z(d) = t_c + t_v$ in (6), rather than being mixed into the compute-side service time.

E.4. Tag-Indexed State Management

KV cache isolation and lifecycle. M_q maintains a mapping from tag to KV cache. When an $M_p^{(i)}$ starts a new decoding session, M_q initializes an empty KV cache entry for its tag; during each iteration, the inference component loads and updates this KV cache to avoid recompilation of historical activations. When the decoding session finishes, the KV cache entry associated with the tag is released to reclaim memory. This tag-indexed management prevents cross-session contamination and enables efficient lookup and update with many active $M_p^{(i)}$. Importantly, this isolation is necessary for

session-conditioned quantities such as $\beta_i(y)$ in (1) and $l_i(d)$ in (2) to remain well-posed, where each return must advance the *same* session prefix and KV state associated with that tag.

Extending to other per- $M_p^{(i)}$ metadata. The same tag-indexed design applies to other per- $M_p^{(i)}$ states maintained at M_q , such as speculative metadata and bookkeeping information required by the execution loop. By enforcing strict per-tag isolation, StarSD preserves correctness under concurrency while keeping M_q scalable in both memory usage and scheduling.

F. Extended GPU Experiment Details

This section supplements the frequency-sensitivity study in Fig. 6(b) by verifying that GPU frequency control is indeed taking effect during our experiments. To verify whether GPU frequency control is effective, we log the measured frequency just before each draft-side inference begins in both the default setting and when the GPU graphics clock is locked.

GPU frequency lock command. We enable persistence mode and lock the graphics clock to 2400 MHz using the following commands:

GPU Frequency Lock Commands

```
sudo nvidia-smi -pm 1
sudo nvidia-smi -i 0 -lrc 2400,2400
```

Unless otherwise specified, the “Default (unlocked)” setting means leaving the GPU in its default DVFS behavior, without applying a fixed graphics clock.

Frequency probing via NVML. After applying the frequency lock or leaving it unlocked for the default setting, we probe the instantaneous graphics clock *immediately before* the draft model starts inference in each iteration. Concretely, we query NVML through pynvml by using the following command:

GPU Frequency Measurement

```
pynvml.nvmlDeviceGetClockInfo(\_gpu\_handle, pynvml.NVML\_CLOCK\_GRAPHICS)
```

We record these measurements for each experimental configuration, which means different numbers of target instances N . In post-processing, we discard spurious outliers where the returned frequency is very low, which can occur during handle initialization or end of string task, and then aggregate the remaining samples to produce the summary shown in Fig. 7.

Observed frequency stability. Figure. 7 confirms that the locked configuration stays at 2400 MHz across all tested N , whereas the default configuration exhibits higher and varying graphics clocks. This verification ensures that the trends reported in Fig. 6(b) are valid.

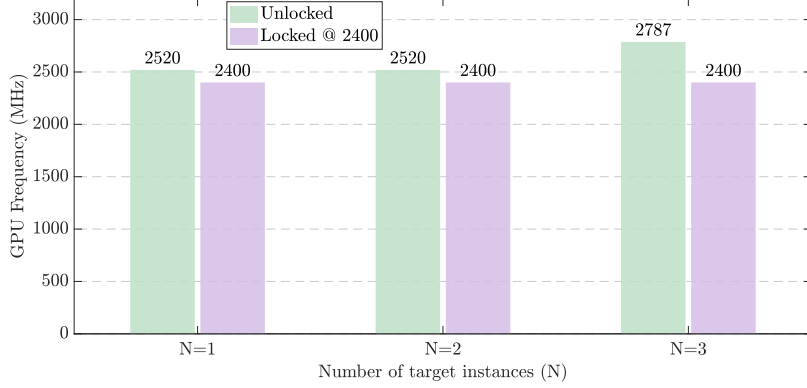


Figure 7. Measured GPU graphics clock frequency before each draft-side inference under the default DVFS setting versus a fixed 2400 MHz lock.

G. Draft Inference Time Under Different Experimental Settings

Draft inference speed We report the draft-side inference time measured during our experiments. To obtain accurate GPU kernel timing under CUDA’s asynchronous execution, we use `torch.cuda.Event(enable_timing=True)` and compute elapsed time via `event.elapsed_time()` with an explicit `torch.cuda.synchronize()` to ensure all kernels have completed.

CUDA Event Timing Snippet

```

starter = torch.cuda.Event(enable_timing=True)
ender = torch.cuda.Event(enable_timing=True)

starter.record()
# draft forward pass
ender.record()

torch.cuda.synchronize()
infer_ms = starter.elapsed_time(ender) # milliseconds

```

Draft inference time trend. Figure. 8 plots the measured draft-side inference time under different numbers of target instances N on RTX 4090 server. As N increases from 1 to 2 or above, the inference time drops markedly, where $N=1$ trace concentrates around ~ 16 ms with pronounced jitter and frequent spikes, whereas the $N=2$ and $N=3$ traces form much tighter bands around ~ 9 ms with only occasional outliers.

Summary statistics. Table 2 summarizes the draft-side inference time. As N increases from 1 to 2-3, the mean inference time decreases substantially and the variance drops sharply, indicating a faster and much more stable draft-side execution.

Table 2. Draft-side inference time statistics.

N	Mean (ms)	Variance (ms 2)
1	16.06	6.34
2	8.86	0.30
3	9.17	0.12

H. Deployment Illustrations

StarSD is designed to support disaggregated speculative decoding across a range of deployment topologies as shown in Fig. 9, from intra-node multi-GPU setups to networked multi-node clusters and heterogeneous edge-server environments.

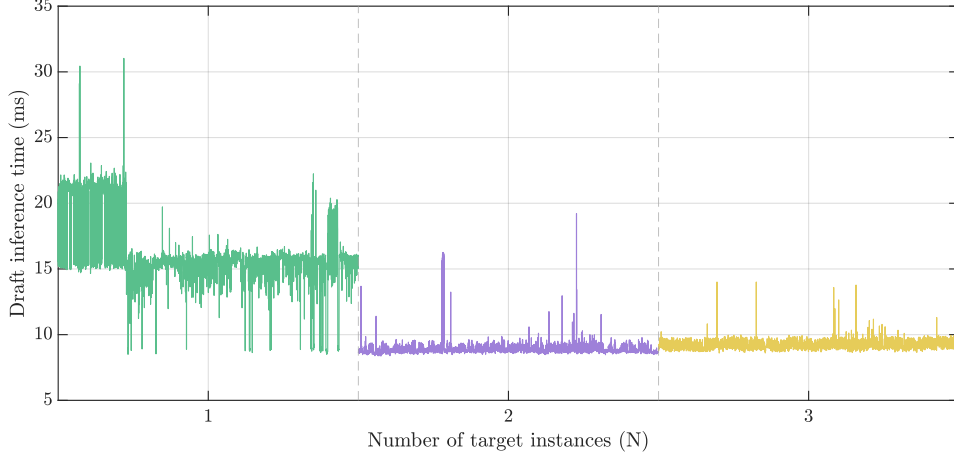


Figure 8. Draft-side inference time under different numbers of target instances N .

To make these supported scenarios explicit, we summarize three representative deployment modes:

- **Intra-Node Multi-GPU (Intra-MG):** *machine-internal cross-GPU* within a single machine.
- **Inter-Node Cluster (Inter-CL):** *cross-machine* deployment over a network.
- **Edge-Server Hybrid (Inter-ES):** *cross-device* deployment (e.g., Jetson-PC) emphasizing heterogeneity and portability.

Demo A: Intra-Node Multi-GPU (Intra-MG). In Intra-MG, the draft server hosting M_q is placed on one GPU, while the target instances $\{M_p^{(i)}\}$ are placed on other GPUs within the same node. A representative configuration is to place M_q on a single GPU and run three target instances on the remaining GPUs of a 4-GPU server. This topology matches the *machine-internal cross-GPU* scenario and is a natural fit when co-locating M_q and $M_p^{(i)}$ on the same device is infeasible due to memory pressure. Since all communication stays within one machine, StarSD can exploit high-bandwidth intra-host GPU transport, e.g., NVLink, to reduce transfer overhead. The real-world setup is shown in Fig. 10(a).

Demo B: Inter-Node Cluster (Inter-CL). In Inter-CL, the draft server and target instances are placed on different machines, corresponding to the *cross-machine* deployment over a network. A representative configuration is to host the draft instance alongside a subset of target instances on a single multi-GPU server, e.g., one GPU for draft and three GPUs for targets, while placing additional target instances on another server equipped with a different GPU type to form a heterogeneous cluster. Because the dataflow must traverse the network, we use a socket-based messaging layer for portability across commodity Ethernet and heterogeneous cluster environments, while keeping the StarSD execution logic unchanged. More specialized transports, e.g., RDMA or cluster-specific collectives, can be integrated as an optimization, but are not required for StarSD to function. The real-world setup is shown in Fig. 10(b).

Demo C: Edge-Server Hybrid (Inter-ES). To demonstrate *cross-device* portability, we also include an edge-server deployment in which one side runs on an embedded edge device, e.g., a Jetson, and the other side runs on a desktop/server GPU machine. This scenario stresses heterogeneous compute capability and network constraints, and therefore uses the same socket-based messaging layer as Inter-CL. The real-world setup is shown in Fig. 10(c).

I. Limitations and Future Directions

Limitations. While StarSD demonstrates that a one-for-many speculative decoding framework can reduce draft-side idle gaps and improve overall utilization, the current design has several limitations.

- **Fairness and per-target quality of service are not explicit goals.** StarSD is primarily optimized for high utilization and aggregate throughput. Without explicit fairness constraints, e.g., per-target rate limits, weighted scheduling, or latency service level objective (SLOs), some targets may experience worse tail latency under contention.

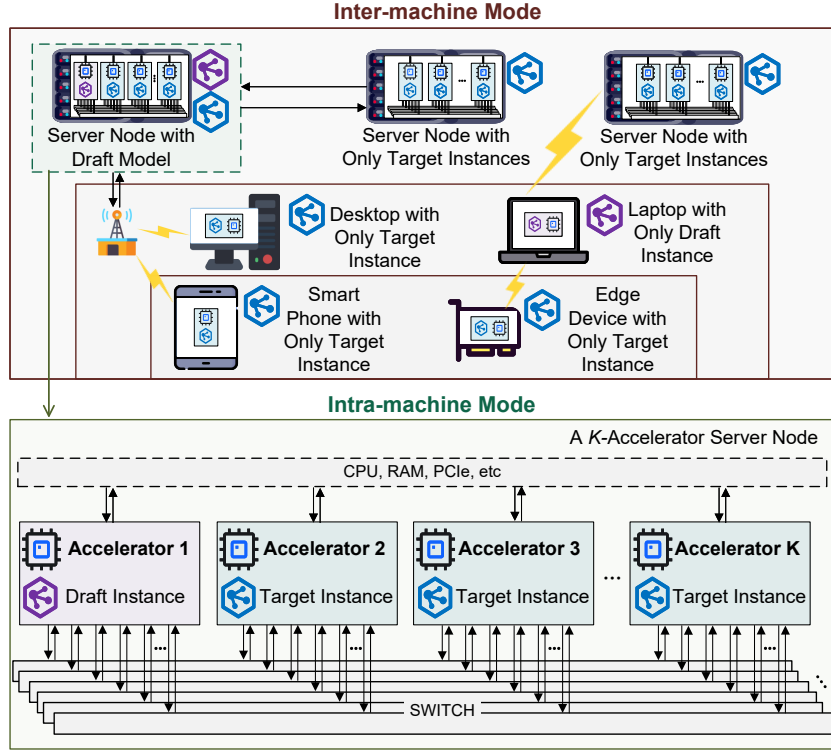


Figure 9. Deployment illustrations for StarSD. (A) **Intra-MG**: draft instance runs on one GPU and serves multiple target instances on other GPUs within the same machine, where communication can leverage intra-machine high-speed GPU interconnects, e.g., NVLink. (B) **Inter-CL**: draft instance runs as a draft server on one machine while target instances are placed on other machines, communication crosses the network boundary and is implemented via socket-based messaging. (C) **Inter-ES**: draft instance runs on one edge device, e.g., a laptop, whereas the target instances run on other edge devices, e.g., NVIDIA Jetson, and communication follows the same Inter-CL setup.

- **State isolation and memory pressure at scale.** Maintaining per-tag KV caches and speculative metadata is necessary for correctness, but it increases the memory footprint at the draft side. With many concurrent sessions, cache growth and fragmentation can reduce effective capacity and complicate eviction policies.
- **Hardware heterogeneity is under-explored.** When targets run on heterogeneous accelerators, e.g., different GPUs or edge devices, the variance in verification time increases, and scheduling becomes more challenging. The current system does not explicitly optimize for heterogeneous service rates or energy trade-offs.

Future directions. We see multiple promising directions to extend StarSD beyond the current one-for- N design.

Toward an M -for- N draft-target fabric. A natural extension is an M -for- N framework, where multiple draft instances $\{M_q^{(j)}\}_{j=1}^{N_q}$ collaboratively serve multiple target instances $\{M_p^{(i)}\}_{i=1}^{N_p}$. Compared with one-for- N , the key objective is to remove the single-draft bottleneck while preserving high utilization and correctness under asynchronous returns. Concretely, this raises several system and algorithmic questions. (i) **Dynamic pairing and load balancing:** route each incoming verified prefix to a suitable draft instance based on queue length, predicted service time, and recent acceptance statistics. (ii) **State placement:** decide whether per-tag KV caches live with a fixed draft instance, migrate across drafts, or reside in a shared cache layer. (iii) **Consistency and replay:** ensure correctness when requests may be retried or migrated across drafts, requiring idempotent protocols and explicit versioning of speculative metadata. (iv) **Scheduling with heterogeneity:** incorporate heterogeneous compute and network costs to achieve both high throughput and bounded tail latency.

Adaptive and learning-based control. Another direction is to make key system parameters adaptive to workload dynamics and latency SLOs, including the speculation depth d , batching policy, and routing strategy. For example, the system can adjust d online using lightweight predictors of acceptance length and verification latency, or learn scheduling policies that

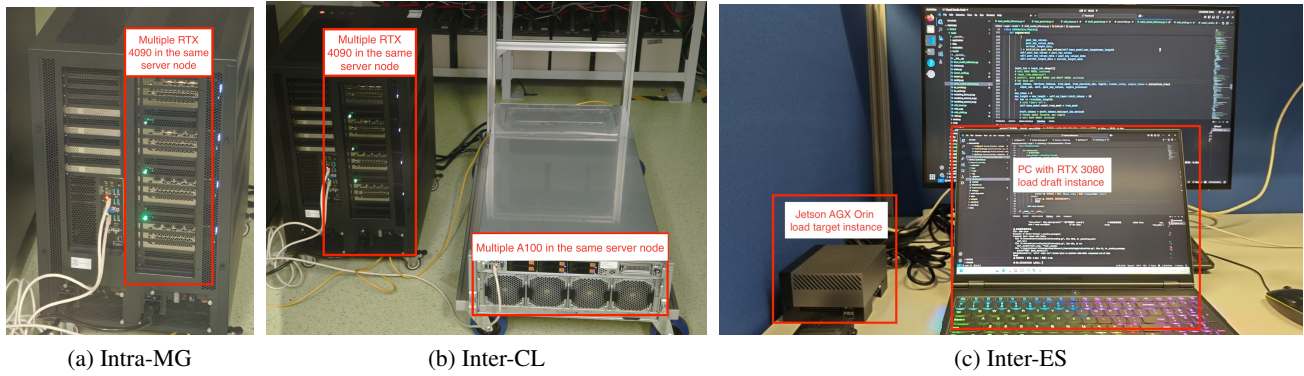


Figure 10. Photograph of the inter-server node deployment, the intra-server node deployment, and the Jetson-PC hybrid deployment.

optimize a multi-objective target, e.g., throughput, latency, fairness, and energy.